MedChemComm

RESEARCH ARTICLE

View Article Online
View Journal

Cite this: DOI: 10.1039/c7md00302a

Cu(II) immobilized on Fe_3O_4@APTMS-DFX nanoparticles: an efficient catalyst for the synthesis of 5-substituted 1*H*-tetrazoles with cytotoxic activity

Faezeh Taghavi,[a] Mostafa Gholizadeh, *[a]
Amir Sh. Saljooghi [a] and Mohammad Ramezani[b]

Cu(II) immobilized on deferasirox loaded amine functionalized magnetic nanoparticles (Cu(II)/Fe_3O_4@APTMS-DFX) as a novel magnetically recyclable heterogeneous catalyst is able to catalyze the [3 + 2] cycloaddition reactions of various organic nitriles with sodium azide. Using this method, a series of 5-substituted-1*H*-tetrazoles under mild conditions in DMSO were prepared. The reaction involves mild reaction conditions with efficient transformation capability. The developed catalyst could be easily separated by applying an external magnetic field. Furthermore, it could be recycled for 5 runs with negligible leaching of copper from the surface of the catalyst. The catalyst was characterized by various techniques such as FT-IR, TGA, VSM, SEM-EDX, and ICP-OES. Several derivatives of 1*H*-tetrazoles were prepared using this catalyst, and their structures were confirmed using different techniques. Then, the synthesized anthraquinones were evaluated for their cytotoxicity against several cell lines including MCF-7, MAD-MD-231, HT-29, HeLa, neuro-2a and L-929. The results obtained from the MTT assay revealed that the 6 derivatives exhibited a high level of cytotoxicity. In order to determine the cytotoxicity mechanism, 2 derivatives with the highest cytotoxic activity were selected, and an apoptosis assay was carried out by flow cytometry, which supported that apoptosis is the major mechanism.

Received 18th June 2017,
Accepted 17th August 2017

DOI: 10.1039/c7md00302a

rsc.li/medchemcomm

1. Introduction

Various catalytic methods for the synthesis of tetrazoles as a class of heterocyclic compounds are currently under immense focus because of their widespread applications. Tetrazoles are used in pharmaceuticals as lipophilic spacers,[1] photography and information recording systems,[2] catalysis technology and high energy chemistry.[3] Tetrazoles are approximately 10-fold more lipophilic than the corresponding carboxylates, which is a useful property for a drug molecule to pass through cell membranes easily.[2] Also, tetrazolic acids are more resistant than carboxylic acids in many metabolic degradation routes.[2] Commonly, 5-substituted 1*H*-tetrazoles are synthesized through reaction of nitriles with hydrazoic acid,[4] trimethylsilyl azide ($TMSN_3$),[5] and sodium azide.[6,7] Among these methods, the [3 + 2] cycloaddition reaction of sodium azide and diverse nitriles is an attractive and common method. Recently, various catalytic systems such as Brønsted acids,[8] Lewis acids including $BF_3{\cdot}OEt_2$,[9] $AlCl_3$,[10] zinc salts,[11] copper triflates,[12] tangstates,[13] and $AgNO_3$,[14] supported catalysts such as SiO_2–H_3BO_3,[15] $NaHSO_4{\cdot}SiO_2$,[16] $FeCl_3{\cdot}SiO_2$,[17] and Fe_3O_4@SiO_2/salen of Cu(II),[18] chitosan derived magnetic ionic liquids,[19] Cu–MCM-41,[20] $WAIPO_5$ based microspheres,[21] clays,[22] Ag NPs,[23] metal oxides such as Cu_2O[24] and ZnO,[25] and alloys like Zn/Cu[26] and Zn/Al hydrotalcites[27] have been reported for the synthesis of tetrazoles. Although all of these catalytic systems are useful, a number of existing methods have some drawbacks such as stringent conditions, expensive reagents, toxic and expensive metal catalysts, long reaction times, low yields of final products, difficulty in the separation and recovery of the catalyst and tedious work-ups.[20] In recent years, heterogeneous catalytic systems have received considerable attention because of their easy separation, recyclability of catalysts and eco-friendly conditions. Recently, magnetic nanomaterials with potential applications in catalysis, biomedicine, biotechnology, materials science and target drug delivery were reported.[28] Magnetic nanoparticles (MNPs) were used as efficient supports for homogeneous catalysts instead of porous materials in organic chemistry.[29] MNP supported catalysts can be easily removed and recycled from the reaction

[a] Department of Chemistry, Faculty of science, Ferdowsi University of Mashhad, P. O. Box 91775-1436, Mashhad, Iran. E-mail: m_gholizadeh@um.ac.ir; Tel: +98 513880 5527
[b] Pharmaceutical Research Center, School of Pharmacy, Mashhad University of Medical Sciences, P. O. Box 91775-1365, Mashhad, Iran

mixture using an external magnet, which is a faster method in comparison with filtration and centrifugation methods, and the catalyst loss can be minimized during the separation. Also, it can increase the purity of the products and moreover improve the operation costs.[30] In order to control the size, shape and magnetic properties of the hybrid materials, the core–shell structures of MNPs have been reported.[31] SiO_2 coated magnetic nanoparticles were prepared and modified with various desirable functional groups for a range of applications such as metal nanoparticle loading for high catalytic activity.[32] Herein, our research group would like to report the preparation of Cu(II) immobilized on Fe_3o_4@APTMS-DFX as a novel heterogeneous catalyst for the preparation of 5-substituted 1*H*-tetrazoles.

2. Experimental

2.1. Chemicals and apparatus

All solvents were purchased from Merck Co. Triethylamine (NEt_3), 4-hydrazino-benzoic acid, and 2-(2-hydroxyphenyl)-4*H*-3,1-benzoxazin-4-one were purchased from Merck without further purification. 1-Ethyl-3-[3-dimethylaminopropyl] carbodiimide hydrochloride (EDC) and 7-hydroxybenzotriazole hydrate (HOBt) were purchased from Fluka (Germany). RPMI-1640 medium, Dulbecco's modified Eagle's medium (DMEM) and fetal bovine serum (FBS) were purchased from GIBCO (Gaithersburg, USA). Penicillin and streptomycin were purchased from Biochrom AG (Berlin, Germany). MTT (3-(4,5-dimethylthiazol-2-yl)-2,5-diphenyltetrazolium bromide, a yellow tetrazole) was purchased from Sigma Co., Ltd. Cisplatin was purchased from Sigma Aldrich. Benzonitrile derivatives, sodium azide, $Cu(OAC)_2$ and (3-aminopropyl) trimethoxysilane (APTMS) were purchased from Sigma Aldrich. NMR spectra were recorded on Avance Bruker-400 MHz spectrometers. All chemical shifts in NMR experiments are reported as ppm and were referenced to residual solvent. Chemical shifts are reported in parts per million, and the signals are denoted as s (singlet), br (broad), d (doublet) and m (multiplet). FT-IR spectra were recorded on an AVATAR-370-FTIR Thermo Nicolet instrument. All mass spectra were scanned using a Varian Mat CH-7 instrument at 70 eV. The reactions were monitored by TLC using silica gel plates, and the products were identified by comparing their spectra and physical data with those of the authentic samples. Melting points were measured using Electrothermal 9100 apparatus. Scanning electron microscopy (SEM) images were taken using a Zeiss LEO 1450 VP/35Kv instrument (Germany). Thermogravimetric analysis (TGA) was carried out using a thermogravimetric analyzer TGA-50 (Shimadzu Japan) instruments. Elemental analysis was carried out using a CHNS (O) Analyzer Model FLASH EA 1112 series (Thermo Finnigan, Italy). Magnetization values were obtained using a vibrating sample magnetometer (VSM, 7400 Lake Shore, America). Inductively coupled plasma optical emission spectrometry (ICP-OES) was carried out using a Varian, VISTA-PRO, CCD (Australia).

2.2. Synthesis of 4-[3,5-bis(2-hydroxyphenyl)-1,2,4-triazol-1-yl] benzoic acid (deferasirox)

2-(2-hydroxyphenyl)-4*H*-3,1-benzoxazin-4-one was synthesized according to a previously reported procedure with some modifications.[33,34] 4-Hydrazinobenzoic acid (11.5 mmol, 1.75 g) and Et_3N (11.5 mmol, 1.16 g) were dissolved in boiling EtOH (80 mL). Then, 2-(2-hydroxyphenyl)-4*H*-3,1-benzoxazin-4-one (10.45 mmol, 2.50 g) was added to the clear solution, and the reaction mixture was refluxed for an additional 2 h. After the completion of the reaction (monitored by TLC), the solution was cooled down to room temperature, and water was added until the first sign of precipitation was observed. The mixture was then concentrated to a total volume of 50% under reduced pressure, and an aqueous 6 M HCl solution (40 mL) was added. The resulting solid was filtered, washed with water and dried for 24 h in a vacuum. Yellow powder; (3.11 g, yield = 80%); m.p. 264–266 °C; IR (KBr) ν: 3317, 2540, 1680 (C=O), 1607, 1517, 1495, 1431, 1351, 1221, 988, 752 cm^{-1}; ^1H NMR (C_3H_6O-d_6 400 MHz): δ 7.00 (s, 1H), 7.01–7.04 (m, 3H), 7.39 (m, 2H), 7.48 (d, 1H), 7.53 (d, 2H), 8.15 (d, 2H), 8.19 (d, 1H) 10.00 (s, OH), 10.78 (s, OH) ppm; ^{13}C NMR (C_3H_6O-d_6, 75 MHz): δ 113.7, 113.9, 116.6 (CH), 117.0 (CH), 119.5 (CH), 119.8 (CH), 124.0 (2 CH), 126.9 (CH), 130.4 (2 CH), 130.5, 130.7 (CH), 131.4 (CH), 132.6, 141.9 (CH), 152.1, 155.6, 156.4, 160.4, 165.7 (C=O) ppm; M.S. (70 eV) *m*/*z* (%): 374 (M+); anal. calc. for $C_{21}H_{15}N_3O_4$: C, 67.56%; H, 4.05%; N, 11.25%. Found: C, 67.76%; H, 3.85%; N, 11.14%.

2.3. Synthesis of Fe_3O_4 NP_S

The magnetite nanoparticles (Fe_3O_4 MNPs) were prepared *via* a previously reported chemical co-precipitation technique with ferric and ferrous ions in alkaline solution, with some modifications.[35,36] $FeCl_2{\cdot}4H_2O$ (9.25 mmol) and $FeCl_3{\cdot}6H_2O$ (15.8 mmol) were dissolved in deionized water (150 mL) under an Ar atmosphere at room temperature. An NH_4OH solution (25%, 50 mL) was then added dropwise (drop rate = 1 mL min^{-1}) to the stirring mixture at room temperature to reach a reaction pH of about 11. The resulting black dispersion was continuously stirred for 1 h at room temperature and then collected using an external magnet.

2.4. Surface modification of Fe_3O_4 MNP by APTMS (MNP@APTMS)

The Fe_3O_4 magnetic nanoparticles were modified with APTMS (MNP@APTMS) according to the previously reported procedure by Lui *et al.*[37] The MNPs were dispersed in 100 mL of methanol/toluene (volume ratio of 1 : 1) as solvent and then sonicated for 30 min and heated up to 95 °C until 50 mL of the solvent was evaporated. Thereafter, methanol (50 mL) was added. The operation was repeated three times to ensure that the solution was completely anhydrous. Subsequently, the volume of the reaction mixture was fixed at 100 mL by the addition of methanol followed by the addition of APTMS and stirring for a certain time (30 or 70 °C under N_2). The product was washed several times with ethanol and distilled

water by magnetic decantation and dried under vacuum. The product was washed with toluene, and Soxhlet extraction was performed for 24 h to remove unreacted APTMS and finally, dried at 40–50 °C for 6 h.

2.5. The functionalization of the APTMS modified MNPs with deferasirox

Deferasirox (4.2 mmol) was dissolved in 100 ml of toluene, which was then added to 1.1 g of the APTMS-modified Fe_3O_4 MNPs in the presence of EDC (50 mg)/HOBt (40 mg) to activate the carboxylate groups of deferasirox for amide bond formation.[38] This mixture was refluxed under stirring for 24 h and was then filtered and washed with 100 ml of dry toluene (Soxhlet extraction) for 24 h. The solid product was dried at room temperature under vacuum. The prepared catalyst was abbreviated as Fe_3O_4@APTMS-DFX.

2.6. Preparation of Cu(II) immobilized Fe_3O_4@APTMS-DFX

Fe_3O_4@APTMS-DFX (1 g) was mixed with Cu $(OAc)_2{\cdot}H_2O$ (0.6 mmol, 0.11 g) and absolute EtOH (5 mL) and stirred at room temperature under an Ar atmosphere for 4 h. The resulting suspension was separated using an external magnet and then dried in an oven at 60 °C for 16 h.

2.7. Typical procedure for the preparation of 5-phenyl-1*H*-tetrazoles

Sodium azide (0.0650 g, 1 mmol), benzonitrile (0.1031 g, 1 mmol), and the catalyst (0.03 g) were mixed and stirred in DMSO (5 mL). The reaction temperature was raised up to 120 °C for 1 h. The progress of the reaction was monitored by thin-layer chromatography (TLC) in ethyl acetate:*n*-hexane. After the completion of the reaction, the catalyst was removed using an external magnet, and the reaction mixture was treated with HCl (4 N, 10 mL) and EtOAc (10 mL). The resultant organic layer was separated, washed with distilled water (2 × 10), dried over anhydrous sodium sulfate, and concentrated to give the crude solid 5-phenyl-1*H*-tetrazole. The crude product was recrystallized in n-hexane/ethyl acetate. The spectral data for selected products are presented as follows:

5-Phenyl-1*H*-tetrazole (Table 2, entry 1). White solid; mp 214–216 °C (Lit.[39] 214–216 °C); FT-IR (KBr): ν_{max}/cm^{-1} 3129, 3054, 2981, 2910, 2701, 2609, 2545, 2481, 1866, 1608, 1563, 1485, 1465, 1409,1290,1258, 1163, 1056, 992, 787, 726, 687 498; ^{1}H NMR (400 MHz, DMSO-d_6, ppm) δ 7.60–7.64 (m, 3H, Ph), 8.02–8.07 (m, 2H, Ph).

5-(4-Chlorophenyl)-1*H*-tetrazole (Table 2, entry 2). White solid, mp 261–262 °C (Lit.[41] 261–263 °C); FT-IR (KBr): ν_{max}/cm^{-1} 3092, 3060, 3007, 2978, 2907, 2851, 2725, 2622, 2537, 2471, 1609, 1564, 1486, 1435, 1160, 1096, 1053, 1020, 990, 833, 745, 508; ^{1}H NMR (400 MHz, DMSO-d_6, ppm) δ 7.68 (d, J = 8.4 Hz, 2H, Ph), 8.05 (d, J = 8.8 Hz, 2H, Ph).

5-(4-Boromophenyl)-1*H*-tetrazole (Table 2, entry 4). White solid, mp 264–265 °C (Lit.[40] 265 °C); FT-IR (KBr): ν_{max}/cm^{-1} 3117, 3089, 3003, 2900, 2846, 2757, 2730, 2639, 2553, 2479, 2308, 2222, 2128, 1604, 1558, 1482, 1430, 1276, 1156, 1119, 1078, 1053, 1017, 990, 874, 829, 743, 691, 502, 452; ^{1}H NMR (400 MHz, DMSO-d_6, ppm) δ 7.83 (d, J = 12 Hz, 2H, Ph), 8.01 (d, J = 12, 2H, Ph).

5-(3,5-Dimethoxyphenyl)-1*H*-tetrazole (Table 2, entry 7). White solid, mp 204–205 °C (Lit.[42] 204–206 °C). FT-IR (KBr): ν_{max}/cm^{-1} 3129, 3064, 3011, 2975, 2941, 2843, 2757, 2712, 2634, 1605, 1562, 1480, 1430, 1287, 1208, 1162, 1167, 1054, 827, 747; ^{1}H NMR (400 MHz, DMSO-d_6, ppm) δ 3.84 (s, 6H, –OMe), 6.72 (t, J = 2 Hz, 1H, Ph), 7.21 (d, J = 2 Hz, 2H, Ph), 16.91(1H, br s, NH).

4-(1*H*-Tetrazol-5-yl) phenol (Table 2, entry 10). White solid, mp 234–236 °C (Lit.[43] 234–235 °C). FT-IR (KBr): ν_{max}/cm^{-1} 3252, 3101, 3066, 3019, 3000–2200, 1615, 1599, 1511, 1466, 1413, 1282, 832, 752, 514; ^{1}H NMR (400 MHz, DMSO-d_6, ppm) d 6.97 (d, J = 8.4 Hz, 2H, Ph), 7.87 (d, J = 8.8 Hz, 2H, Ph), 10.20 (2H, br s, OH).

Table 1 Optimization of the model reaction over the Cu(II)/Fe_3O_4@APTMS-DFX nanocatalyst

Entry	Molar ratio (nitrile : NaN_3)	Catalyst (g)	Solvent	Temperature (°C)	Time (h)	Isolated yield (%)
1	1 : 1	—	DMSO	120	24	30
2[a]	1 : 1	0.03	DMSO	120	1	—
3	1 : 1	0.001 (0.1 mol%)	DMSO	120	9	35
4	1 : 1	0.02 (1.5 mol%)	DMSO	120	3	80
5[b]	1 : 1	0.03 (2.5 mol%)	DMSO	120	24	40
6	1 : 1	0.03 (2.5 mol%)	DMSO	120	1	98
7	1 : 1	0.03 (2.5 mol%)	DMSO	110	1	80
8	1 : 1	0.03 (2.5 mol%)	DMSO	100	1	70
9	1 : 1	0.03 (2.5 mol%)	DMSO	130	1	98
10	1 : 1	0.05 (4 mol%)	DMSO	130	1	98
11	1 : 1	0.03 (2.5 mol%)	—	120	1	25
12	1 : 1	0.03 (2.5 mol%)	DMF	120	1	65
13	1 : 1	0.03 (2.5 mol%)	H_2O	120	1	Trace
14	1 : 1	0.03 (2.5 mol%)	CH_3CN	120	1	30
15	1 : 1	0.03 (2.5 mol%)	EtOH	120	1	70
16	1 : 1.5	0.03 (2.5 mol%)	DMSO	120	1	98
17[c]	1 : 1	0.03 (2.5 mol%)	DMSO	120	1	75

[a] The reaction was performed in the presence of Fe_3O_4@APTMS-DFX. [b] The reaction was carried out in the presence of **IV**. [c] The reaction was accomplished in the presence of $Cu(OAC)_2{\cdot}H_2O$.

Table 2 Scope of the Cu(II)/Fe_3O_4@APTMS-DFX promoted tetrazole synthesis of various substrates

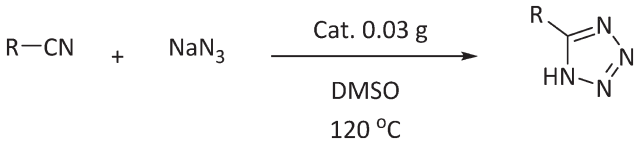

Entry	Substrate	Product	Time (h)	Isolated yield (%)
1	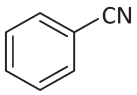	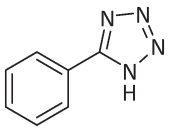	1	98
2	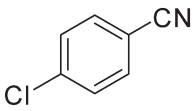	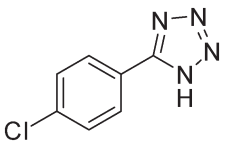	1.5	95
3	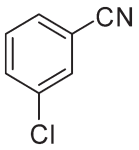	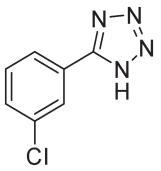	1.5	93
4	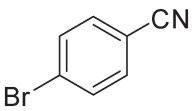	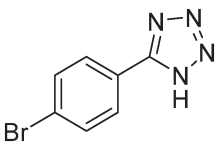	2.5	92
5	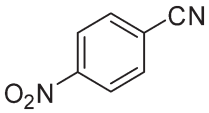	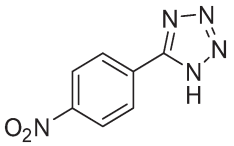	1	98
6	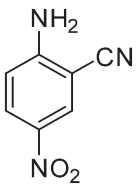	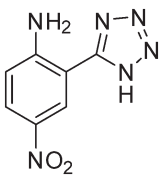	2.5	90
7	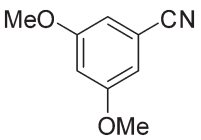	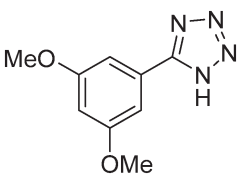	4	85
8	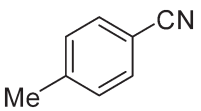	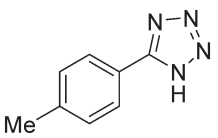	3.5	83
9	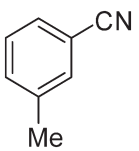	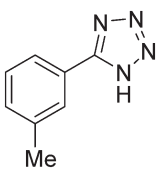	4	80
10	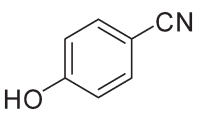	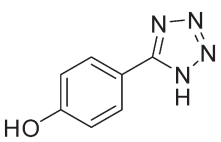	5	80

Table 2 *(continued)*

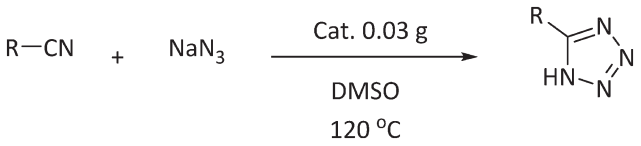

Entry	Substrate	Product	Time (h)	Isolated yield (%)
11	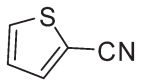	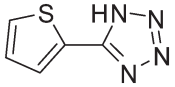	2	80
12	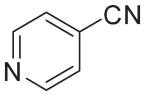	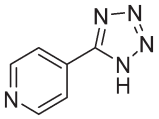	1	95
13	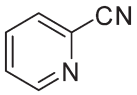	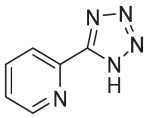	1.5	93
14	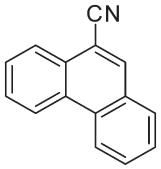	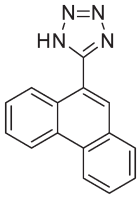	4	88
15	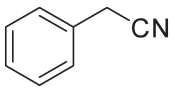	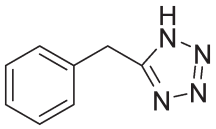	5	75
16	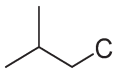	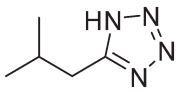	6	74
17	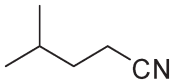	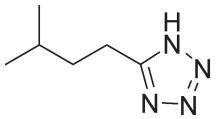	5	77

5-(Thiophen-2-yl)-1*H*-tetrazole (Table 2, entry 11). White solid, mp 206–207 °C (Lit.[44] 205–207 °C). FT-IR (KBr): ν_{max}/cm^{-1} 3109, 3074, 2974, 2891, 2780, 2722, 2628, 2569, 2500, 2456, 1830, 1595, 1503, 1411, 1233, 1139, 1046, 962, 853, 740, 719; ^{1}H NMR (400 MHz, DMSO-d$_6$, ppm) δ 7.29–7.32 (m, 1H, Thiophen), 7.82 (dd, J = 6, 1 Hz, 1H, thiophen) 7.90 (dd, 1 Hz, 1H, thiophen).

2-(1*H*-Tetrazol-5-yl) pyridine (Table 2, entry 13). White solid, mp 212–214 °C (Lit.[41] 210–213 °C). FT-IR (KBr): δ_{max}/cm^{-1} 3088, 3060, 2959, 2929, 2864, 2737, 2692, 2622, 2582, 1728, 1602, 1557, 1483, 1449, 1405, 1284, 1158, 1068, 1024, 955, 795, 743, 726, 703, 637, 496; ^{1}H NMR (400 MHz, DMSO-d$_6$, ppm) δ 7.65 (s, 1H, Py), 8.10 (s, 1H, Py), 8.24 (d, J = 6.4 Hz, 1H, Py), 8.81 (s, 1H, Py).

3. Results and discussion

The present study has reported the synthesis of Cu(II) immobilized on Fe_3O_4@APTMS-DFX. In the first step, the Fe_3O_4 MNPs were modified with APTMS, and then deferasirox was conjugated to the surface primary amine groups of the modified MNPs *via* amidation reaction. Finally, Cu(II) ions were anchored onto the deferasirox moiety as a chelating group present on the surface of the catalyst to obtain Cu(II)/Fe_3O_4@APTMS-DFX (Scheme 1). The final catalyst was thoroughly characterized by various spectroscopy and microscopy methods, such as FT-IR, TGA, SEM-EDS and ICP-OES analyses.

3.1. Characterization of Cu(II)/Fe_3O_4@APTMS-DFX

Fig. 1 shows the FT-IR spectrum of the as-synthesized Cu(II)/Fe_3O_4@APTMS-DFX. Fig. 1(a) shows a broad peak around 580 cm^{-1} attributed to the stretching vibration of Fe–O bonds for the uncoated Fe_3O_4 MNPs.[45] Fig. 1(b) for Fe_3O_4@APTMS shows the characteristic peak of Fe_3O_4, which was shifted to 597 cm^{-1}. The peaks at 1030 and 935 cm^{-1} were attributed to the stretching vibration of the Si–O bonds. C–N stretching

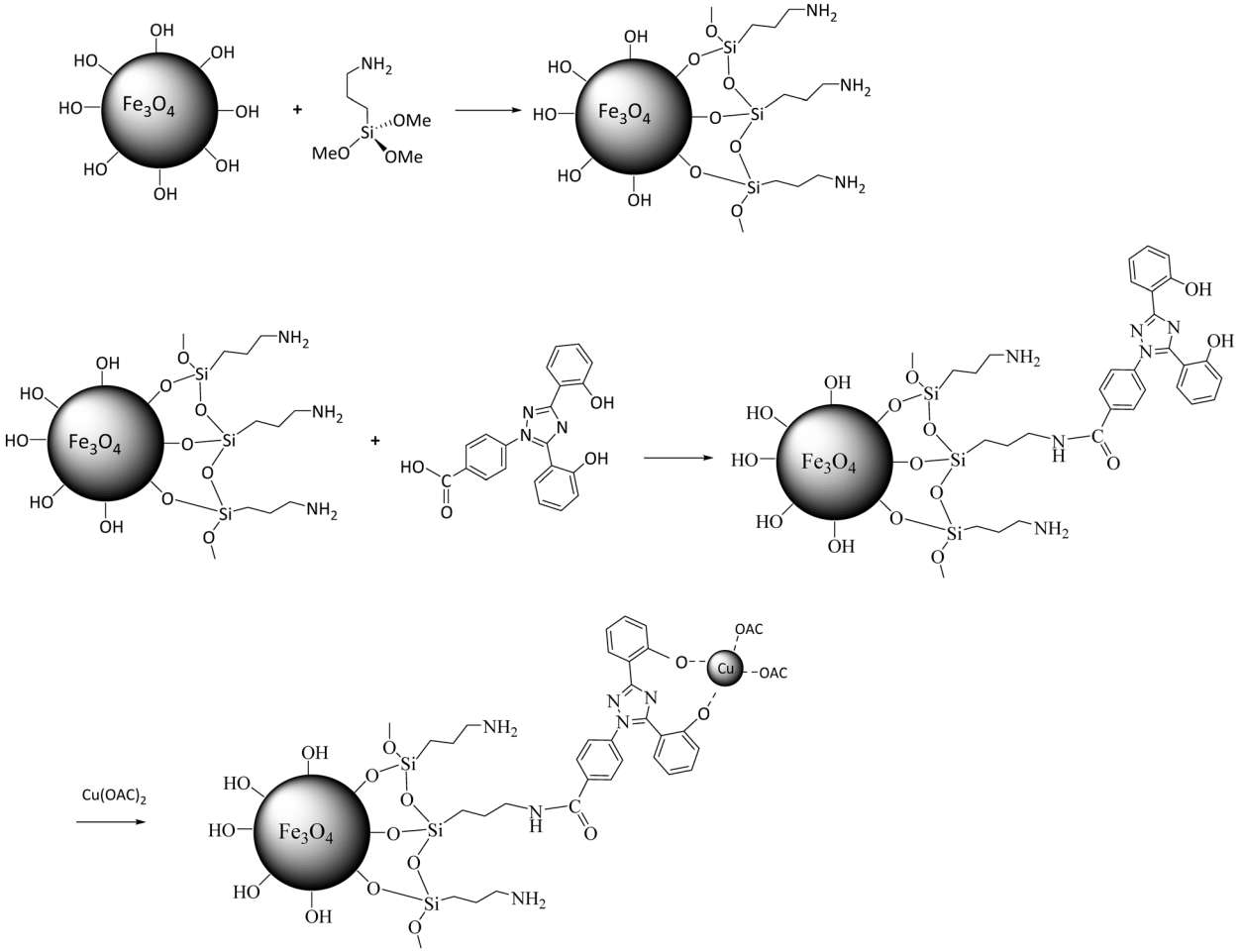

Scheme 1 Preparation procedure of the Cu(II) immobilized on Fe_3O_4@APTMS-DFX.

vibration and N–H bending vibration peaks appeared at 1150 and 1550 cm^{-1}, repectively.[46] The peaks around 2910 cm^{-1} and 3430 cm^{-1} could be attributed to the stretching vibrations of CH_2 and NH_2 groups, respectively. The FT-IR spectrum of Fe_3O_4@APTMS-DFX (Fig. 1(c)) indicates new peaks at 1462, 1605, and 1683 cm^{-1}, which are due to the stretching vibration of the aromatic C=C and C=N of deferasirox. Also, the stretching vibration of the amide carbonyl groups appeared at 1710 cm^{-1}. C–H stretching of aromatic systems and propyl groups was observed at 2921–3100 cm^{-1}. The broad absorption peak at 3435 cm^{-1} could be attributed to the O–H groups of deferasirox and the N–H stretching band of the amide groups. Fig. 1(d) shows the absorption band at 450 cm^{-1}, which was attributed to the Cu–O vibration of Cu(II)/Fe_3O_4@APTMS-DFX. All the observed peaks revealed that the surface of the Fe_3O_4 NPs was successfully modified with organic moieties and Cu(II) ions were loaded onto the modified surface of the catalyst, which were in agreement with the results reported in the literature.[47]

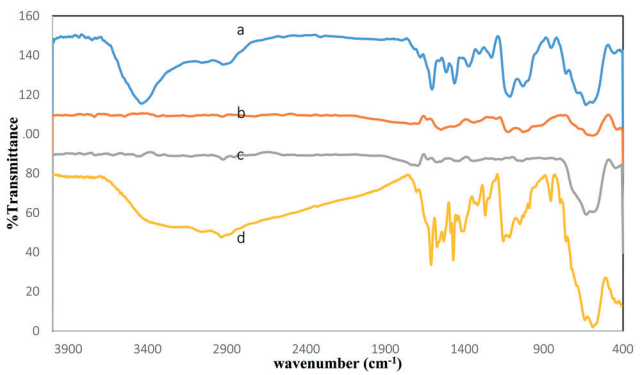

Fig. 1 FTIR spectra of (a) the magnetic nanoparticles (MNPs), (b) 3-(aminopropyl)trimethoxysilane modified MNPs (MNP@APTMS), (c) deferasirox anchored on MNP@APTMS (MNP@APTMS-DFX) and (d) Cu(II)/Fe_3O_4@APTMS-DFX.

To investigate the thermal stability of the catalyst, thermogravimetric analysis was performed. Fig. 2(a) shows the typical TGA curve of MNP@APTMS. The initial weight loss up to 250 °C was probably due to the removal of surface hydroxyl groups and/or surface adsorbed water molecules. The weight loss at 250–500 °C could be attributed mainly to the evaporation and subsequent decomposition of surface bonded APTMS. The Fe_3O_4 MNPs can transform to Fe_2O_3 and the weight would increase when the temperature is above 500 °C. As shown in Fig. 2(b), the weight loss of Fe_3O_4@APTMS-

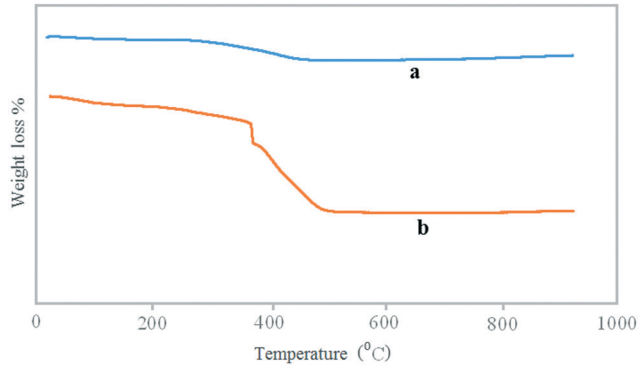

Fig. 2 TGA curve of (a) MNP@APTMS and (b) MNP@APTMS-DFX.

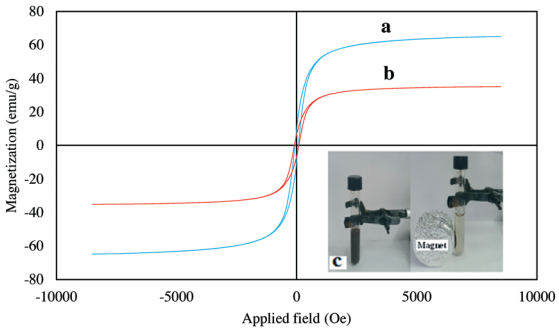

Fig. 4 Magnetization curve of (a) bare Fe_3O_4 and (b) Fe_3O_4@APTMS-DFX. (c) Photograph of the separation of magnetic nanoparticles with an external magnet.

DFX is much higher than that of Fe_3O_4@APTMS in the temperature range of 250–500 °C, which confirms the modification of the Fe_3O_4 surfaces with organic DFX and APTMS Species.

The morphology of the Fe_3O_4 nanoparticles before and after deferasirox loading was studied by scanning electron microscopy (SEM). As shown in Fig. 3(a) and (b), the nanoparticles had a small size with a uniform spherical shape. The energy dispersive spectrum (EDS) revealed the presence of Fe, O, C, Si, N and Cu elements (Fig. 3c). These results confirmed that the magnetic nanoparticles were modified using Cu(II)/APTMS-DFX species. The ICP-OES analysis of the catalyst resulted in a value of 5.23 wt% of Cu.

The magnetic properties of the prepared MNPs were investigated *via* vibrating sample magnetometry (VSM). The magnetic hysteresis loops of Fe_3O_4 and Fe_3O_4@APTMS-DFX are shown in Fig. 4. The saturation magnetization (M_s) values at room temperature were 64.9 emu g^{-1} and 35.1 emu g^{-1}, respectively. The M_s value of Fe_3O_4@APTMS-DFX was much lower than that of the Fe_3O_4 MNPs due to the silica coating and DFX loading, providing a smaller magnetic moment per unit mass than that of ferromagnetic core regions and leading to the decreased M_s value. As shown in Fig. 4c, a dark homogeneous dispersion was observed in the absence of an external magnetic field, while in the presence of a magnet, black nanoparticles were adsorbed on the wall of the tube resulting in a transparent solution.

The efficiency of the synthesized Cu(II)-DFX-APTMS@Fe_3O_4 nanocatalyst was investigated for the synthesis of tetrazoles. As a model reaction, the condensation of sodium azide and benzonitrile was carried out in the presence of the as-synthesized catalyst. For the optimization of the reaction conditions, various parameters such as the reaction temperature, catalyst amount and solvent were investigated as shown in Table 1. The main product was obtained only in 30% yield when the reaction was carried out without the catalyst in DMSO as a solvent at 120 °C (Table 1, entry 1). For the reaction performed in the presence of Fe_3O_4@APTMS-DFX as the catalyst, no desired product was formed (Table 1, entry 2).

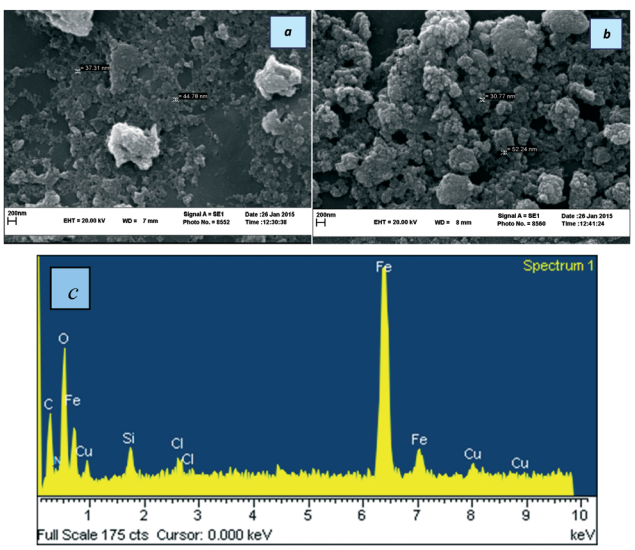

Fig. 3 SEM images of (a) MNP@APTMS and (b) Fe_3O_4@APTMS-DFX and (c) EDS spectrum of Cu(II)/Fe_3O_4@APTMS-DFX.

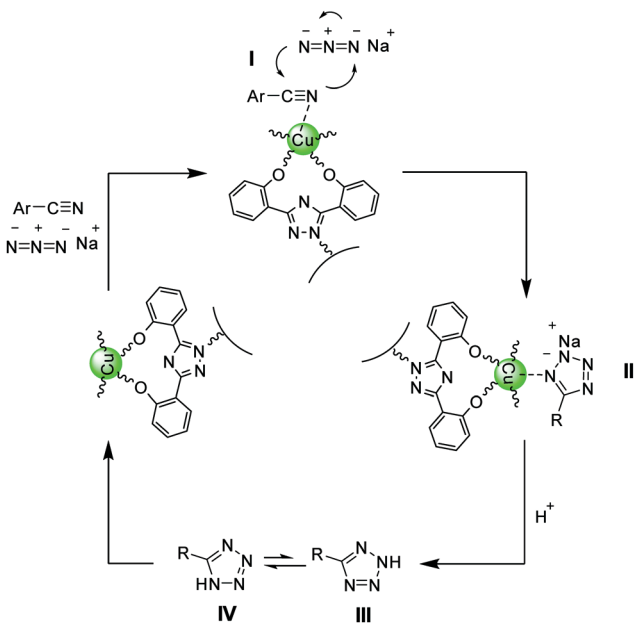

Scheme 2 Plausible mechanism for the synthesis of 5-substituted-1*H*-tetrazoles.

Table 3 Comparison of various catalysts in the synthesis of 5-phenyl-1*H*-tetrazole

Entry	Catalysts	Solvent	Temperature (°C)	Time (h)	Yield (%)	TON	Ref.
1	Imidazole-based zwitterionic-type	—	120	12	84	—	48
2	Mesoporous ZnS	DMF	120	36	96	2.15	49, 55
3	Cu–MCM-41	DMF	140	9	92	—	50
4	Zn/Al-HT	DMF	120	12	84	—	51
5	Amberlyst-15	DMSO	85	12	92	—	52
6	Nano–ZnO	DMF	120	14	72	1.54	53, 55
7	$CuFe_2O_4$	DMF	120	12	82	2.05	54, 55
8	ZnO nanoflake	DMF	125	14	87	1.77	55
9	Cu(II)/Fe_3O_4@APTMS-DFX	DMSO	120	1	98	39.7	This work

Under the same reaction conditions, 98% yield was achieved after 1 h in the presence of 0.03 g of Cu(II)/Fe_3O_4@APTMS-DFX nanocatalyst (Table 1, entry 6). Different solvents such as DMF, H_2O, CH_3CN, and EtOH were tested in the presence of 0.03 g catalyst at the reflux temperature (Table 1, entries 12–15). Based on these results, DMSO was chosen as the suitable solvent for the synthesis of tetrazoles. In the following study, the reaction was carried out in DMSO as a solvent at 120 °C in the presence of different catalyst amounts (0.02 g, 0.03 g, and 0.05 g). With increasing the catalyst amount up to 0.05 g, no significant increase in the yield of main product was observed (Table 1, entry 10). Therefore, 0.03 g of the catalyst and DMSO as the solvent at 120 °C were chosen as the optimized conditions.

The versatility of the optimized conditions for the synthesis of tetrazole derivatives was also investigated (Table 2). The synthesis of various benzonitrile derivatives and sodium azide in DMSO at 120 °C in the presence of 0.03 g of the catalyst was studied. Both electron-withdrawing and electron-donating substituted aromatic benzonitriles were converted to the desired products in excellent yields (Table 2 entries 1–14). Based on these results, aromatic nitriles with electron withdrawing groups (Table 2, entries 2–6, 14) reacted faster than the electron donating analogs (Table 2, entries 7–10). Additionally, heteroaromatic nitriles were also converted to the corresponding tetrazoles in high yields (Table 2, entries 11–13). The cycloaddition reactions of aliphatic nitriles proceeded more slowly than the cycloaddition reactions of aromatic nitriles due to the ineffectiveness of nitriles with electron donating alkyl groups (Table 2, entries 15–17).

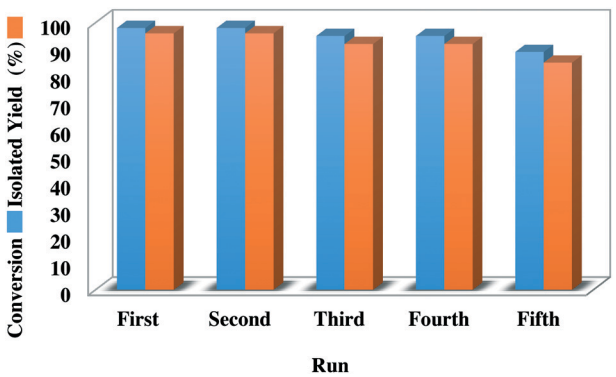

Fig. 5 Recyclability of Cu(II)/Fe_3O_4@APTMS-DFX nanocatalyst.

The plausible mechanistic pathways for the Cu(II)/Fe_3O_4@APTMS-DFX catalyzed tetrazole synthesis reaction are shown in Scheme 2. In the first step, the coordination of the nitrogen atoms of nitriles with Cu(II) forms compound **I** which facilitates the cyclization step and enhances the electrophilic properties of nitriles. Then, it can react with sodium azide *via* [3 + 2] cycloaddition reaction to form intermediate **II**. Acidic work up gives **III** and **IV**. The equilibrium leads to the formation of the more stable tautomer **IV** (5-substituted-1*H*-tetrazole). The efficiency of our method was compared with that using previously reported heterogeneous catalysts in the literature (Table 3). According to these results, all previously reported protocols suffer from long reaction times to obtain appropriate yields, expensive and toxic metals, and tedious purification of products. The Cu(II)/Fe_3O_4@APTMS-DFX nanocatalyst gave higher yield than the other heterogeneous catalysts in shorter reaction time. The recyclability of the Cu(II)/Fe_3O_4@APTMS-DFX nanocatalyst was studied in the model reaction. The results showed that the catalyst had good recyclability with easy recovery and was used for at least 5 consecutive runs without a significant decrease in the product yield (Fig. 5).

4. Biological studies

4.1. Cell culture methods

Human breast cancer cells MDA-MD-231 (ATCC HTB-26)and MCF-7 (ATCC HTB-22), human cervix epithelial carcinoma HeLa (ATCC CCL-2), human colon cancer cell line HT-29 (ATCC HTB-38), mouse neuroblastoma cell line neuro-2a (ATCC CCL-131), and mouse fibroblast L-929 cell line (ATCC CCL-1) were obtained from the American Type Culture Collection (ATCC; Manassas, VA, USA) and cultured at 37 °C in a humidified atmosphere of 5% CO_2 in air. HeLa cells were cultured in Dulbecco's Modified Eagle's Medium (DMEM) with 0.1 mM nonessential amino acids, 2 mM L-glutamine, 1.0 mM sodium pyruvate and 5% fetal bovine serum, at 37 °C in an atmosphere of 5% CO_2. The cells were plated into 96-well sterile plates at a density of 1×10^4 cells per well in 100 μL of the medium and incubated for 24 h. MDA-MD-231, HT-29, MCF-7 and neuro-2a were cultured in DMEM containing 10% fetal bovine serum, 100 units per ml of penicillin and 100 μg ml^{-1} of streptomycin. L-929 cells were cultured in RPMI-1640

Table 4 The IC_{50} values in various cell lines for the synthesized compounds

$IC_{50} \pm SD$ (μM)[a]						
Compound	MCF-7	MDA-MB-231	HT-29	HeLa	Neuro-2a	L-929
1	19.8 ± 3.23	5.77 ± 1.85	18.3 ± 2.83	43.2 ± 5.57	84.2 ± 9.29	>100
2	46.2 ± 5.7	29.6 ± 2.32	20.0 ± 2.86	35.2 ± 4.7	>100	>100
4	58.1 ± 5.23	47.2 ± 4.70	56.4 ± 5.36	65.1 ± 5.35	>100	>100
7	54.3 ± 4.68	4.29 ± 1.98	66.8 ± 5.03	45.5 ± 4.11	95.3 ± 9.70	>100
9	65.2 ± 7.88	39.6 ± 3.29	85.3 ± 6.41	57.9 ± 5.53	87.1 ± 7.53	>100
11	16.9 ± 2.61	15.08 ± 4.27	21.6 ± 4.55	39.1 ± 4.51	98.9 ± 6.80	>100
Cisplatin	5.86 ± 1.47	23.5 ± 4.71	19.5 ± 3.46	0.47 ± 0.13	>100	0.8 ± 0.2

[a] $IC_{50} > 100$ μM is considered to be inactive.

medium containing 10% fetal bovine serum, 100 units per ml of penicillin and 100 μg ml^{-1} of streptomycin.

4.2. Cytotoxicity assay in cancer cell lines

Synthesized compounds were screened for their cytotoxic activity against human breast cancer cells (MDA-MD-231), human cervix epithelial carcinoma (HeLa), human colon cancer cell line (HT-29), human breast cancer cells (MCF-7), mouse neuroblastoma cell line (neuro-2a), and mouse fibroblast L-929 cell line. Cisplatin was used as a comparative positive control. Cell viability was evaluated by using a colorimetric method based on the tetrazolium salt MTT ([3-(4,5-dimethylthiazol-2-yl)-2,5-diphenyltetrazolium bromide]), which is reduced by living cells to yield purple formazan crystals. The cells were seeded in 96-well plates at a density of 2–5 × 10^4 cells of MDA-MD-231, MCF-7, HeLa, HT-29, neuro-2a and L-929 per well in 200 μL of culture medium and left overnight for optimal adherence. After careful removal of the medium, 200 μL of a dilution series of the compounds in fresh medium were added, and incubation was performed at 37 °C in 5% CO_2 for 72 h. Compounds **1**, **2**, **4**, **7**, **9** and **11** were first solubilized in DMSO, diluted in medium and added to the cells in the final concentrations between 20 nM and 200 μM. The percentage of DMSO in cell culture medium did not exceed 0.3%. Cisplatin was first solubilized in saline and then added at the same concentrations used for other compounds. At the end of the incubation period, the medium was removed and the cells were incubated with 200 μL of MTT solution (500 μg ml^{-1}). After 3–4 h at 37 °C in 5% CO_2, the medium was removed and the purple formazan crystals were dissolved in 200 μL of DMSO by shaking. The cell viability was evaluated by the measurement of the absorbance at 570 nm using a STAT FAX-2100 microplate reader (Awareness Technology, Palm City, FL, USA). The cell viability was calculated by dividing the absorbance of each well by that of the control wells (cells treated with medium containing 1% DMSO).

Each experiment was repeated at least three times and each point was determined in at least three replicates. All the synthesized compounds exhibited remarkable cytotoxic activity against cancer cell lines as shown in Table 4. In some cases, their IC_{50} values were lower than those of cisplatin as a popular anti-cancer drug indicating better anti-tumor effects. An interesting issue came into sight was that among the investigated compounds, two derivatives, **7** and **11**, displayed the best results in terms of cytotoxicity. It seems that the presence of methoxy groups play a decisive role in the exhibition of cytotoxic effects. Cytotoxic activity was simultaneously measured for mouse fibroblast normal cell line (L-929) as the control. As shown in Table 4, compounds **1**, **2**, **4**, **7**, **9** and **11** displayed less cytotoxic activity than those against cancer cell lines making them appropriate candidates for anti-cancer drugs. A notable point is that in the case of cisplatin, the IC_{50} value against normal cell L-929 was so low that it was impossible to make a distinction between normal and cancer cells.

The IC_{50} values in all cell lines were measured for the synthesized compounds as well as for cisplatin as a comparative control. The measurements were carried out after 72 h of incubation using the concentrations of the compounds in the range between 20 nM and 200 μM. The determined values of IC_{50} for the compounds spanned between 4.29 and up to 100 μM, while those found for cisplatin as the comparative

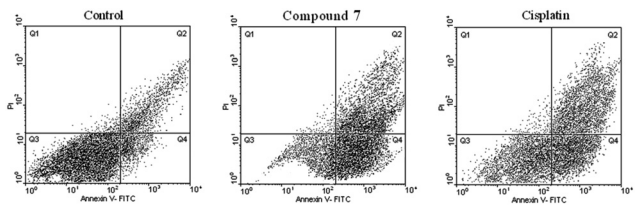

Fig. 6 Flow cytometric results after the exposure of MDA-MB-231 cancer cells to compound **7** and cisplatin. Four areas in the diagrams represent four different cell states: necrotic cells (Q1), late apoptotic or necrotic cells (Q2), living cells (Q3) and apoptotic cells (Q4).

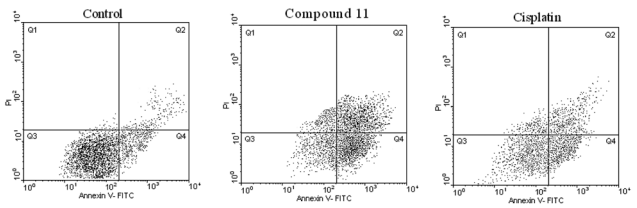

Fig. 7 Flow cytometric results after the exposure of MDA-MB-231 cancer cells to compound **11** and cisplatin. Four areas in the diagrams represent four different cell states: necrotic cells (Q1), late apoptotic or necrotic cells (Q2), living cells (Q3) and apoptotic cells (Q4).

Table 5 Percentage of the cell death by either apoptosis or necrosis pathways observed by flow cytometry for compound 7

Treatment	% Vital cells	% Apoptotic cells	% Late apoptotic/necrotic cells	% Necrotic cells
Control	81.13	8.68	9.45	0.74
Cisplatin	33.74	33.65	31.63	0.98
Compound 7	19.75	44.91	34.54	0.80

Table 6 Percentages of the cell death by either apoptosis or necrosis pathways observed by flow cytometry for compound 11

Treatment	% Vital cells	% Apoptotic cells	% Late apoptotic/necrotic cells	% Necrotic cells
Control	77.5	17.8	3.6	1.1
Cisplatin	34.1	30.8	27.3	7.8
Compound 11	24.2	37.6	31.7	6.5

standard ranged between 0.47 and up to 100 μM (Table 4). Our results indicate that the highest toxicity was observed in the MDA-MB-231 cell line.

4.3. Apoptosis assay for compounds 7 and 11 by flow cytometry

In order to study the mechanism of cell toxicity of compounds **1**, **2**, **4**, **7**, **9** and **11** (necrosis or apoptosis), flow cytometry analysis was performed on the synthesized compounds and cisplatin as a reference. These compounds were incubated for 24 h at a concentration close to the IC_{50} value, and the results are shown in Fig. 6 and 7. Four areas of the diagrams stand for necrotic cells (Q1, low Annexin V-FITC and high PI signal, left square on the top), late apoptotic or necrotic cells (Q2, high Annexin V-FITC and high PI signal, right square on the top), live cells (Q3, low Annexin V-FITC and low PI signal, left square at the bottom), and apoptotic cells (Q4, high Annexin V-FITC and low PI signal, right square at the bottom), respectively. As shown in Fig. 5 and 6 and Tables 5 and 6, compounds 7 and **11** could induce apoptosis in MDA-MB-231 cancer cells. However, the pro-apoptotic properties need further investigation to better understand the precise mechanism of action of the tested compounds.

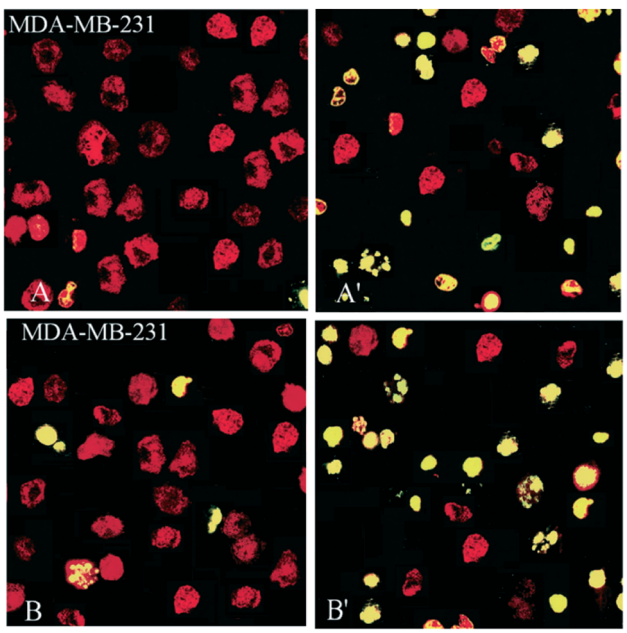

Fig. 8 Compounds **7** and **11** induce apoptosis in the human breast (MDA-MB-231) cancer cell line. The MDA-MB-231 breast cancer (A and A' for **7** and B and B' for **11**) cells were incubated with 10 μM of **7** and **11** for 24 h, fixed, permeabilized and visualized for DNA degradation in a TUNEL assay using dUTP-labeling. Red fluorescence: nuclei stained with propidium iodide. Green or yellow (*i.e.*, superimposed red and green) fluorescence: apoptotic nuclei containing fragmented DNA. When compared with the controls, treated with 0.3% DMSO (A and B), several cells incubated with compounds **7** and **11** (A' and B') exhibited apoptotic nuclei.[56,57]

Compound 7 showed a high population of apoptotic cells (79.45%), nearly 1.2-fold higher than cisplatin (65.28%) at the same concentration (Fig. 6 and Table 5). Besides, according to Fig. 7 and Table 6, compound **11** exhibited a high population of apoptotic cells (69.3%), nearly 1.2 fold higher than cisplatin (58.1%) at the same concentration against the MDA-MB-231 cancer cells.

The cell death induced by the synthesized compounds was also confirmed to be apoptotic using the TUNEL assay of exposed 3'-OH termini of DNA with dUTP-FITC. As shown in the confocal laser scanning microscopy images in Fig. 8, compound-treated MDA-MB-231 breast cancer cells, examined for dUTP-FITC incorporation (green fluorescence) and propidium iodide counterstaining (red fluorescence), exhibited many apoptotic yellow nuclei (superimposed green and red fluorescence) at 24 h after treatment.

The results demonstrated that the newly synthesized compounds could induce apoptosis in the MDA-MB-231 cancer cell line. However, the pro-apoptotic activity needs further investigation to better understand the precise mechanism of action of these compounds. Animal study is needed before they could be recommended for clinical trials.

5. Conclusion

In summary, an efficient catalyst has been developed using Cu(II) immobilized on Fe_3O_4@APTMS-DFX for the preparation of 5-substituted 1*H*-tetrazoles derivatives as important biologically active heterocyclic compounds from nitriles and sodium

azide. The Cu(II)/Fe_3O_4@APTMS-DFX nanocatalyst catalyzed the [3 + 2] cycloaddition reaction of aromatic nitriles and sodium azide giving tetrazoles in excellent to good yields, with short reaction times and easy work up. The developed nanocatalyst can be easily separated using an external magnet and reused for at least 5 times without the loss of its catalytic activity. The results demonstrated that the newly synthesized compounds could induce apoptosis in the MDA-MB-231 cancer cell line. But the pro-apoptotic activity needs further investigation to better understand the precise mechanism of action of these compounds, followed by animal study, before they could be recommended for human clinical trials.

Conflicts of interest

The authors declare no competing interest.

Acknowledgements

The authors gratefully acknowledge the partial support of this study (Grant No: 3/41256) by Ferdowsi University of Mashhad Research Council. We are grateful for help provided by the Buali Research Institute, School of Pharmacy, Mashhad University of Medical Sciences, Mashhad, Iran.

Notes and references

1 G. F. Holland and J. N. Pereira, *J. Med. Chem.*, 1967, **10**, 149–154.
2 R. J. Herr Biorg, *Med. Chem.*, 2002, **10**, 3379–3393.
3 D. P. Curran, S. Hadida and S. Y. Kim, *Tetrahedron*, 1999, **55**, 8997–9006.
4 B. Gutmann, J. P. Roduit, D. Roberge and C. O. Kappe, *Angew. Chem., Int. Ed.*, 2010, **49**, 7101–7105.
5 D. Amantini, R. Beleggia, F. Fringuelli, F. Pizzo and L. Vaccaro, *J. Org. Chem.*, 2004, **69**, 2896–2898.
6 A. N. Chermahini, A. Teimouri, F. Momenbeik, A. Zarei, Z. Dalirnasab, A. Ghaedi and M. Roosta, *J. Heterocycl. Chem.*, 2010, **47**, 913–922.
7 D. Patil, M. Deshmukh and D. Dalal, *J. Iran. Chem. Soc.*, 2012, **9**, 799–803.
8 (*a*) S. H. Watterson, Z. Xiao, D. S. Dodd, D. R. Tortolani, W. Vaccaro, D. Potin, M. Launay, D. K. Stetsko, S. Skala and P. M. Davis, *J. Med. Chem.*, 2010, **53**, 3814–3830; (*b*) S. Takale, S. Manave, K. Phatangare, V. Padalkar, N. Darvatkar and A. Chaskar, *Synth. Commun.*, 2012, **42**, 2375–2381; (*c*) Z. Du, C. Si, Y. Li, Y. Wang and J. Lu, *Int. J. Mol. Sci.*, 2012, **13**, 4696–4703.
9 A. Kumar, R. Narayanan and H. Shechter, *J. Org. Chem.*, 1996, **61**, 4462–4465.
10 D. P. Matthews, J. E. Green and A. J. Shuker, *J. Comb. Chem.*, 2000, **2**, 19–23.
11 Z. P. Demko and K. B. Sharpless, *J. Org. Chem.*, 2001, **66**, 7945–7950.
12 L. Bosch and J. Vilarrasa, *Angew. Chem., Int. Ed.*, 2007, **46**, 3926–3930.
13 J. He, B. Li, F. Chen, Z. Xu and G. Yin, *J. Mol. Catal. A: Chem.*, 2009, **304**, 135–138.
14 P. Mani, A. K. Singh and S. K. Awasthi, *Tetrahedron Lett.*, 2014, **55**, 1879–1882.
15 M. Parveen, F. Ahmad, A. M. Malla and S. Azaz, *New J. Chem.*, 2015, **39**, 2028–2041.
16 B. Das, C. R. Reddy, D. N. Kumar, M. Krishnaiah and R. Narender, *Synlett*, 2010, **3**, 391–394.
17 M. Nasrollahzadeh, Y. Bayat, D. Habibi and S. Moshaee, *Tetrahedron Lett.*, 2009, **50**, 4435–4438.
18 F. Dehghani, A. R. Sardarian and M. Esmaeilpour, *J. Organomet. Chem.*, 2013, **743**, 87–96.
19 A. Khalafi-Nezhad and S. Mohammadi, *RSC Adv.*, 2013, **3**, 4362–4371.
20 M. Abdollahi-Alibeik and A. Moaddeli, *New J. Chem.*, 2015, **29**, 2116–2122.
21 D. Kong, Y. Liu, J. Zhang, H. Li, X. Wang, G. Liu, B. Li and Z. Xu, *New J. Chem.*, 2014, **38**, 3078–3083.
22 M. Abdollahi-Alibeik and M. Pouriayevali, *Catal. Commun.*, 2012, **22**, 13–18.
23 P. Mani, C. Sharma, S. Kumar and S. K. Awasthi, *J. Mol. Catal. A: Chem.*, 2014, **392**, 150–156.
24 T. Jin, F. Kitahara, S. Kamijo and Y. Yamamoto, *Tetrahedron Lett.*, 2008, **49**, 2824–2827.
25 M. Lakshmi Kantam, K. B. S. Kumar and C. Sridhar, *Adv. Synth. Catal.*, 2005, **347**, 1212–1214.
26 G. Aridoss and K. K. Laali, *Eur. J. Org. Chem.*, 2011, **2011**, 6343–6353.
27 M. L. Kantam, K. B. Shiva Kumar and K. Phani Raja, *J. Mol. Catal. A: Chem.*, 2006, **247**, 186–188.
28 V. Polshettiwar and R. S. Varma, *Tetrahedron*, 2010, **66**, 1091–1097.
29 (*a*) D. Lee, J. Lee, H. Lee, S. Jin, T. Hyeon and B. M. Kim, *Adv. Synth. Catal.*, 2006, **348**, 41–46; (*b*) C. O. Dalaigh, S. A. Corr, Y. Gunko and S. J. Connon, *Angew. Chem., Int. Ed.*, 2007, **46**, 4329–4332; (*c*) Y. Zheng, P. D. Stevens and Y. Gao, *J. Org. Chem.*, 2006, **71**, 537–542; (*d*) S. Ding, Y. Xing, M. Radosz and Y. Shen, *Macromolecules*, 2006, **39**, 6399–6405.
30 S. Sobhani and R. Jahanshahi, *New J. Chem.*, 2013, **37**, 1009–1015.
31 (*a*) L. Levy, Y. Sahoo, K. S. Kim, E. J. Bergey and P. N. Prasad, *Chem. Mater.*, 2002, **14**, 3715–3721; (*b*) S. Sacanna, L. Rossi and A. P. Phillipse, *Langmuir*, 2007, **23**, 9974–9982; (*c*) A. Xia, J. Hu, C. Wang and D. Jiang, *Small*, 2007, **3**, 1811–1817.
32 F. Dehghani, A. R. Sardarian and M. Esmaeilpour, *J. Organomet. Chem.*, 2013, **743**, 87–96.
33 R. Lattmann and P. Acklin, *PCT Int. Appl.*, WO9749395A1 Novartis Pharma AG, 1997; Chem. Abstr., 1998, 128, 114953e.
34 Y. I. Ryabukhin, L. N. Faleeva and V. G. Korobkova, *Chem. Heterocycl. Compd.*, 1983, **19**, 332–336.
35 R. Massart, E. Dubois, V. Cabuil and E. Hasmonay, *J. Magn. Magn. Mater.*, 1995, **149**, 1–5.
36 B. Z. Tang, Y. Geng, J. W. Y. Lam, B. Li, X. Jing, X. Wang, F. Wang, A. B. Pakhomov and X. X. Zhang, *Chem. Mater.*, 1999, **11**, 1581–1589.

37 G. Y. L. Lui, P. Obeidy, S. J. Ford, C. Tselepis, D. M. Sharp, P. J. Jansson, D. S. Kalinowski, Z. Kovacevic, D. B. Lovejoy and D. R. Richardson, *Mol. Pharmacol.*, 2013, **83**, 179–190.
38 Z. Salmasi, W. T. Shier, M. Hashemi, E. Mahdipour, H. Parhiz, K. Abnous and M. Ramezani, *Eur. J. Pharm. Biopharm.*, 2015, **96**, 76–88.
39 V. Aureggi and G. Sedelmeier, *Angew. Chem., Int. Ed.*, 2007, **46**, 8440–8444.
40 S. Lossen and J. Liebigs, *Ann. Chem.*, 1897, **298**, 101–102.
41 V. Rama, K. Kanagaraj and K. Pitchumani, *J. Org. Chem.*, 2011, **76**, 9090–9095.
42 B. Sreedhar, A. S. Kumar and D. Yadav, *Tetrahedron Lett.*, 2011, **52**, 3565–3569.
43 T. Jin, F. Kitahara, S. Kamijo and Y. Yamamoto, *Tetrahedron Lett.*, 2008, **49**, 2824–2827.
44 A. Najafi Chermahini, A. Teimouri and A. Moaddeli, *Heteroat. Chem.*, 2011, **22**, 168–173.
45 S. Mohapatra, N. Pramanik, S. Mukherjee, S. K. Ghosh and P. J. Pramanik, *Mater. Sci.*, 2007, **42**, 7566–7574.
46 M. Shen, H. Cai, X. Wang, X. Cao, K. Li, S. H. Wang, R. Guo, L. Zheng, G. Zhang and X. Shi, *Nanotechnology*, 2012, **23**, 105601–105610.
47 M. Esmaeilpour, J. Javidi, F. Nowroozi and M. Mokhtari, *J. Mol. Catal. A: Chem.*, 2014, **393**, 18–29.
48 M. Rahman, A. Roy, M. Ghosh, Sh. Mitra, A. Majee and A. Hajra, *RSC Adv.*, 2014, **4**, 6116–6119.
49 (*a*) L. Lang, B. Li, W. Liu, L. Jiang, Z. Xu and G. Yin, *Chem. Commun.*, 2010, **46**, 448–450; (*b*) L. Lang, H. Zhou, M. Xue, X. Wang and Z. Xu, *Mater. Lett.*, 2013, **106**, 443–446.
50 M. Abdollahi Alibeika and A. Moaddeli, *New J. Chem.*, 2015, **39**, 2116–2122.
51 M. L. Kantam, K. B. Shiva Kumar and K. J. Phani Raja, *J. Mol. Catal. A: Chem.*, 2006, **247**, 186–188.
52 R. Shelkar, A. Singh and J. Nagarkar, *Tetrahedron Lett.*, 2013, **54**, 106–109.
53 M. Lakshmi Kantam, K. B. S. Kumar and C. Sridhar, *Adv. Synth. Catal.*, 2005, **347**, 1212–1214.
54 B. Sreedhar, A. S. Kumar and D. Yada, *Tetrahedron Lett.*, 2011, **52**, 3565–3569.
55 E. Erkena, I. Esirdenb, M. Kaya and F. Sen, *RSC Adv.*, 2015, **5**, 68558–68564.
56 R. K. Narla, Y. Dong, O. J. D'Cruz, C. Navara and F. M. Uckun, Bis (4,7-dimethyl-1,10-phenanthroline) Sulfatooxovanadium (IV) as a Novel Apoptosis-inducing Anticancer Agent, *Clin. Cancer Res.*, 2000, **6**, 1546–1556.
57 D. M. Zhu, R. K. Narla, W. H. Fang, N. C. Chia and F. M. Uckun, Protection against hydrogen peroxide-mediated cytotoxicity in Friedreich's ataxia fibroblasts using novel iron chelators of the 2-pyridylcarboxaldehyde isonicotinoyl hydrazone class, *Clin. Cancer Res.*, 1998, **4**, 2967–2976.

